Title
A hybrid origin of the Martian crustal dichotomy: Degree-1 convection antipodal to a giant impact

Authors
Citron, Robert I
Manga, Michael
Tan, Eh

Publication Date
2018-06-01

DOI
10.1016/j.epsl.2018.03.031

Peer reviewed

A hybrid origin of the Martian crustal dichotomy: Degree-1 convection antipodal to a giant impact

Robert I. Citron[ab] Michael Manga[ab] Eh Tan[c]

Abstract

The Martian crustal dichotomy is the stark ~5 km difference in surface elevation and ~26 km difference in crustal thickness between the northern lowlands and southern highlandsthat originated within 100s of Myr of Mars' formation. The origin of the dichotomy has broad implications for the geodynamic history of Mars, but purely exogenic or endogenic theories so far cannot explain all of the large scale geophysical observations associated with dichotomy formation. A giant impact can produce the shape and slope of the dichotomy boundary, but struggles to explain Mars' remanent crustal magnetic signatures and the ultimate formation of Tharsis. Degree-1 mantle convection can relate the crustal dichotomy to the formation of Tharsis, but does not explain the elliptical dichotomy shape and must be initiated by a large pre-existing viscosity jump in the mantle. We propose a hybrid model of dichotomy formation in which a giant impact induces degree-1 convection with an upwellingantipodal to the impact site. In this scenario, a giant impact in the northern hemisphere excavates crust, creating an initial difference in crustal thickness and possibly composition between the two hemispheres. Over 10s to 100s of Myr, the dominant upwelling(s) would migrate to be under the thicker, insulating crust in the southern hemisphere, generating melt that further thickens the southern crust. We examine this process using 3-D mantle convection simulations, and find that a hemispherical difference in crustal thickness and composition caused by a giant impact can induce degree-1 convection with the upwelling(s) antipodal to the impact site in <100 Myr.

Keywords: Mars, geodynamics, mantle convection, planetary evolution

1. Introduction

1.1. Constraints on dichotomy formation

One of the oldest observable features on Mars is the crustal dichotomy, an approximately hemispheric difference of ~5 km in surface elevation and ~26 km in crustal thicknessbetween the northern lowlands (Borealis basin) and southern highlands (*e.g.*, Neumann et al., 2004). The formation of the dichotomy is generally attributed to either an exogenic event such as a giant impact (*e.g.*, Marinova et al., 2008), or an endogenic process such as mantleconvection (*e.g.*, Roberts and Zhong, 2006). There are several important constraints or potential constraints on the formation mechanism, including the timing of dichotomy formation, boundary shape, magnitude of variation in crustal thickness, distribution/strength of remanent crustal magnetism (residual magnetization retained in crustal rocks after cessation of the dynamo), and formation of Tharsis on the dichotomy boundary.

Crater retention ages for buried and visible craters suggest that the dichotomy likely originated within 100s of Myrs of Mars' formation (*e.g.*, Frey, 2006), and geochemical arguments also suggest an early formation time ~4.5 Ga (Bottke and Andrews-Hanna, 2017; Brasser and Mojzsis, 2017). Relatively early formation of the dichotomy is consistent with a giant impact during the late stages of planetary accretion (Brasser and Mojzsis, 2017), but limits endogenic theories because it constrains the timescale for mantle convection to evolve to a degree-1 pattern. Solid–solid phase changes in the mantle have been successful at producing degree-1 convection, but only on Gyr timescales and require a constant or weakly temperature dependent viscosity (Harder, 2000; Roberts and Zhong, 2006). Degree-1 convection can arise on shorter timescales (100s of Myr) if Mars had a temperature dependent, layered viscosity with a factor of 25 increase in the mid-mantle (Roberts and Zhong, 2006). It is unclear what process would cause such a large viscosity jump in the mantle, but it could be the result of a solid–solid phase transition, compositional variation from an early magma ocean, or a transition from diffusion to dislocation creep (*e.g.*, Roberts and Zhong, 2006). Compositional layering due to magma ocean solidification has been proposed as a mechanism to generate asymmetrical overturn on timescales <10 Myr (*e.g.*, Elkins-Tanton et al., 2005), however, more recent work has shown that degree-1 structures are unlikely to result from mantle overturn on Mars (Scheinberg et al., 2014).

The elliptical shape of the dichotomy boundary has been used as evidence for a giant impact because Borealis-scale impacts produce elliptical basins due to the effects of planet curvature (Andrews-Hanna et al., 2008) and the scale of the impact (Collins et al., 2011). An elliptical basin could also be the result of an impact megadome, which occurs when an impact is large enough to cause widespread crust production and magmatism in the impacted hemisphere, a scenario that could potentially result in a Borealis-like depression in the hemisphere opposite the megadome (*e.g.*, Golabek et al., 2018). An elliptical boundary shape would not be an expected result of degree-1 convection, but migration of a single upwelling and the resulting crust production could result in asymmetries in the dichotomy boundary (Šrámek and Zhong, 2012). An elliptical dichotomy shape could result from one-ridge convection, where the upwelling planform is a single ridge spread over half of Mars (Keller and Tackley, 2009). Furthermore, although the dichotomy boundary appears elliptical, the pre-Tharsis boundary computed by removing Tharsis depends on the elastic plate thickness (Andrews-Hanna et al., 2008) and contributions of lateral or temporal elastic thickness variations are unexplored (Šrámek and Zhong, 2010).

The extent of crustal thickness variation between the northern and southern hemispheres of Mars, as inferred from gravity and topography data (*e.g.*, Neumann et al., 2004), is possible with both exogenic and endogenic dichotomy formation mechanisms. Coupling of melt/crust production with mantle convection models can produce crust in one hemisphere of similar thickness to the present-day highlands (Šrámek and Zhong, 2012; Keller and Tackley, 2009), however, such crust production depends on the vigor of convection and not all plumes produce melt (Sekhar and King, 2014). The required crustal thickness variation can also be produced by magmatism resulting from an impact megadome (Golabek et al., 2011). For a Borealis-scale impact, numerical impact simulations show that the resulting crustal thickness variation is generally consistent with present observations (Marinova et al., 2008; Nimmo et al., 2008). An additional effect of excavating crust in the northern hemisphere via a giant impact is the formation of a circum-Mars debris disk that could explain the formation of the Martian moons Phobos and Deimos (*e.g.*, Rosenblatt et al., 2016). The sharp dichotomy boundary expected from an impact could also induce edge driven convection, possibly explaining the buried mass anomalies on the eastern dichotomy boundary (Kiefer, 2005).

Another constraint on dichotomy formation is the remanent crustal magnetic signatures that are observed over the entire planet, indicating another global process active early in Martian history (Acuna et al., 1999). The remanent magnetic signatures are significantly stronger in the southern hemisphere, and also contain a unique pattern of lineations of alternating polarity (Connerney et al., 2005). The emplacement of the magnetic signatures most likely occurred prior to the cessation of the Martian dynamo ~4.1 Ga (Lillis et al., 2013), although it is uncertain if the magnetic signatures were emplaced before, during, or after dichotomy formation. The magnetic signatures must post-date a giant impact because a Borealis-scale impact could have completely erased magnetic signatures in the northern lowlands, and the thick ejecta blanket could have demagnetized the entire southern crust as well (Citron and Zhong, 2012). Even if an impact occurred in the presence of a strong magnetic field, the pattern of magnetic lineations of alternating polarity is difficult to reconcile with Borealis-scale impact/ejecta generated melt or magmatism associated with an impact megadome (*e.g.*, Golabek et al., 2018), which would have cooled on a short timescale in the vertical direction. The alternating polarity of the lineations could be explained by crust production radiating from a single large plume in a reversing magnetic field, which might explain why the geometry of the lineations roughly corresponds to concentric circles centered around a single pole that is <300 km from the centroid of the thickened southern crust (Citron and Zhong, 2012). However, the melting history is likely more complex than the simple model of Citron and Zhong (2012), and could involve multiple migrating plumes and more complex melt extraction and crust evolution. Furthermore, the pattern of lineations observed from orbit does not necessarily represent the distribution of magnetized material at depth. Still, emplacement of the magnetic signatures during thickening of the southern crust could at least explain the higher strength and concentration of remanent magnetic signatures in the southern hemisphere, particularly if degree-1 convection promotes the development of a hemispherical dynamo (Stanley et al., 2008).

The formation of Tharsis on the dichotomy boundary also favors the endogenic theory of dichotomy formation. If degree-1 convection sufficiently thickens the southern crust, it would create a layer of highly viscous melt residue under the thickened crust. This lateral variation in viscosity could cause differential rotation of the lithosphere or migration of the degree-1 upwelling, until the plume reaches the dichotomy boundary and creates Tharsis (Zhong, 2009; Šrámek and Zhong, 2010, Šrámek and Zhong, 2012). Plume migration from the south pole to Tharsis' location is supported by observations of volcanic resurfacing, demagnetization, and increased crustal thickness along that path (Hynek et al., 2011; Cheung and King, 2014), and is consistent with the creation of Tharsis within a few hundred Myrs of dichotomy formation (*e.g.*, Nimmo and Tanaka, 2005, and references therein).

1.2. A hybrid origin

Neither a purely exogenic nor endogenic model can easily or obviously explain all geophysical observations related to dichotomy formation. Because of this, we examine a hybrid model in which a giant impact forms the Borealis basin, producing an initial nearly hemispherical difference in crustal thickness and composition that induces degree-1 convection with the upwelling centered under the thicker, enriched (in radiogenic-heat producing elements) crust opposite the impact site (Fig. 1). Although initially an upwelling should develop under the impact site, such an upwelling should dissipate relatively quickly (*e.g.*, Roberts and Arkani-Hamed, 2017), allowing for the composition and structure of the crust/lithosphere to control the convection pattern over longer timescales (100s of Myr). We expect the northern and southern post-impact crusts to differ in composition, specifically the concentration of radiogenic-heat producing elements, because of the depletion of such elements from the mantle over time. During Mars' initial crust formation, radiogenic-heat producing elements would be partitioned into the crust, creating an ancient crust enriched in such elements and depleting the mantle of the same elements. The giant impact would strip the northern hemisphere of its original, enriched crust, and the new crust in the northern hemisphere would be derived from an already depleted mantle, resulting in a new northern crust that is depleted in radiogenic-heat producing elements relative to the southern crust. The compositional difference between the newer depleted crust in the northern hemisphere and the ancient crust in the southern hemisphere could persist for billions of years (Ruedas and Breuer, 2017). On early Mars, the thicker, enriched crust in the hemisphere opposite the impact should have an insulating effect that increases the mantle temperature and promotes hot spot and plume formation under the thicker, enriched southern crust, similar to the effect of supercontinents on Earth (*e.g.*, Gurnis, 1988). In this scenario, the initial crustal thickness variation caused by the Borealis impact is not as extensive as currently observed, but is amplified by the additional melt produced by the superplume that naturally develops in the southern hemisphere due to the insulating southern crust. New crust production in the southern hemisphere could explain the formation of the remanent crustal magnetic signatures (provided that the crust is produced before the end of the dynamo), and could also result in a layer of highly viscous melt residue. The melt residue under the southern crust could induce plume migration and/or differential lithosphere rotation resulting in the formation of Tharsis on the dichotomy boundary (Zhong, 2009; Šrámek and Zhong, 2010).

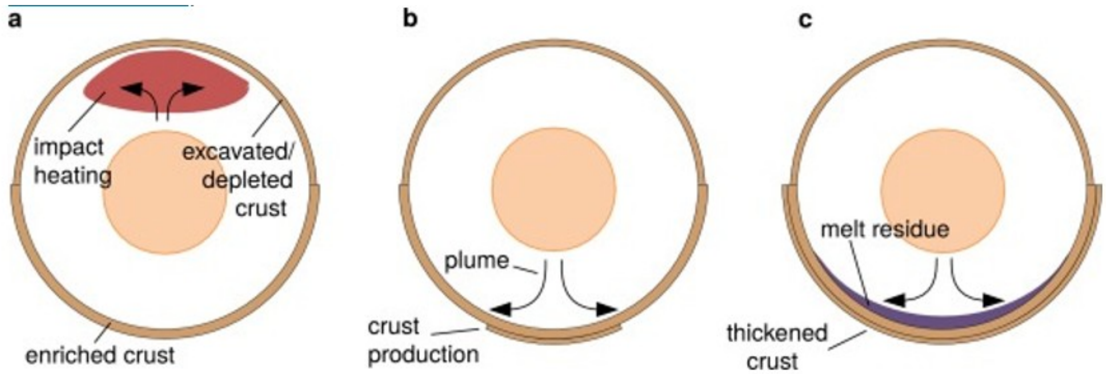

Fig. 1. (a) An impact causes excavation, heating, and a transient upwelling in the northern hemisphere. While a new northern crust would form relatively rapidly, it would form from an already depleted mantle(depleted from forming the original crust) and thus be depleted in radiogenic-heat producing elements relative to the older, more enriched southern crust (Ruedas and Breuer, 2017). (b) The insulating effect of the thicker, enriched southern crust results in degree-1 convection with a large upwelling in the southern hemisphere. (c) Melt generation from the upwelling(s) further thickens the crust in the hemisphere opposite the impact, and resulting melt residue could explain subsequent migration of the plume/lithosphere and the formation of Tharsis at the dichotomy boundary (Zhong, 2009).

Degree-1 convection has previously been shown to migrate so that the upwelling becomes centered under an insulating cap (Šrámek and Zhong, 2010), however, these simulations relied on a large viscosity jump (*e.g.*, Roberts and Zhong, 2006) to initiate degree-1 convection without the presence of an insulating cap. Because a possible mechanism for a large mid-mantle viscosity jump, a transition from ringwoodite to a basal perovskite/ferropericlase layer, likely occurs in the deepest mantle or not at all on Mars (*e.g.*, Ruedas et al., 2013), crustal thickness and composition may be more important factors in Martian mantle dynamics. Crustal structure has been shown to have an important effect on mantle convection on present-day Mars (Plesa et al., 2016), and experiments suggest that upwellings could have focused under an insulating lid on early Mars (Wenzel et al., 2004). In this study, we examine if degree-1 convection forms on Mars as a natural response to an impact-generated insulating cap with no viscosity jump in the mid-mantle, and with the upwelling centered in the hemisphere opposite the impact site. We conduct numerical simulations of mantle convection for a range of initial crustal thickness variations and insulating effects.

2. Methods

Mantle convection simulations are conducted using CitcomS (Zhong et al., 2000; Tan et al., 2006), a finite element mantle convection code widely used in studies of Earth and other planetary bodies. The Martian mantle is represented by a spherical shell heated from below and within using the Boussinesq approximation, given by the following non-dimensional governing equations:

$$(1)\quad \nabla\cdot\mathbf{u}=0$$

$$(2)\quad -\nabla P+\nabla\cdot[\eta(\nabla\mathbf{u}+\nabla^{T}\mathbf{u})]+RaT\mathbf{e}_r=0$$

$$(3)\quad \frac{\partial T}{\partial t}+\mathbf{u}\cdot\nabla T=\nabla\cdot(\kappa(r)\nabla T)+H_{int}-H_L$$

where **u**, *P*, *T*, and *η* are the velocity vector, pressure, temperature, and viscosity, respectively, and $\kappa(r)$ is a non-dimensional prefactor for the thermal diffusivity to account for a reduced thermal conductivity in the crust. The latent heating rate from magma melting is H_L. The Rayleigh number *Ra* is defined as

$$(4)\quad Ra=\frac{\rho_m g\alpha_0\Delta T R_p^3}{\kappa_0\eta_0}$$

where R_p is the planetary radius, *g* is gravitational acceleration, ΔT is the super-adiabatic temperature difference, and ρ_m, α_0, κ_0, and η_0 are the reference values for mantle density, thermal expansivity, thermal diffusivity, and viscosity, respectively. The reference viscosity corresponds to the value at the base of the mantle. The internal heating number H_{int} is defined as

$$(5)\quad H_{int}=\frac{QR_p^2}{\rho_m C_p\Delta T\kappa_0}$$

where C_p is the specific heat at constant pressure and *Q* is a variable volumetric heating rate based on Wanke and Dreibus (1994) that decays with time (starting at 50 Myr after solar system formation). We allow for cooling of the core based on the heat flux from the bottom boundary (*e.g.*, Plesa et al., 2016, and references therein):

$$(6)\quad C_c\rho_c V_c\frac{dT_{CMB}}{dt}=-q_c A_c$$

where we assume an adiabatic core with constant specific heat capacity $C_c=800\ \mathrm{J\,K^{-1}\,kg^{-1}}$ and density $\rho_c=7200\ \mathrm{kg\,m^{-3}}$, q_c is the heat flux from the core, and V_c and A_c are the volume and surface area of the core, respectively.

For simplicity, we use the Boussinesq approximation, neglecting adiabatic heating/cooling and instead adding an adiabatic gradient to the simulation temperature before computing melting (Li et al., 2016). The effect of using the Boussinesq approximation instead of the extended Boussinesq approximation should be small due to the low dissipation number for Mars (Plesa and Breuer, 2014). Although our simplification could affect the amount of melting, it should not affect the convective pattern and significantly alter our main conclusions.

The Martian mantle may deform via either diffusion or dislocation creep. We use a non-dimensional pressure- and temperature-dependent viscosity similar to Roberts and Zhong (2006) but with no viscosity layering prefactor:

$$(7)\quad \eta=\eta_0\exp\left(\frac{E'+V'(1-r)}{T+T_s}+\frac{E'+V'(1-R_c)}{1+T_s}\right)$$

where *r* is the non-dimensional radius, and the non-dimensional parameters E', V', and T_s, and non-dimensional temperature *T*, are given by

$$(8)\quad E'=\frac{E_a}{R\Delta T},\quad V'=\frac{\rho_m g R_p V_a}{R\Delta T},\quad T_s=\frac{T_{surf}}{\Delta T},\quad T=\frac{T_d}{\Delta T}-T_s$$

where E_a, V_a, *R*, and T_{surf} are the activation energy, activation volume, gas constant, and surface temperature, respectively, and T_d is the dimensional temperature.

The simulation is composed of 12 spherical caps, each with a resolution of $64\times64\times64$ elements, with an increasing radial resolution near the boundary layers. We use isothermal, free-slip boundary conditions on the top and bottom boundaries. We use the parameters listed in Table 1 and an initial non-dimensional mantle temperature $T_m=0.75$, with top/bottom thermal boundary layers determined by a conductive half-space cooling/heating model (error function) with a time of 50 Myr. We start the simulation with random perturbations of 0.01 to the non-dimensional temperature in the mid-mantle.

Table 1. Model parameters.

Parameter	Symbol	Value
Planetary radius	R_p	3400 km
Core radius	R_c	1650 km
Gravitational acceleration	g	3.73 $\mathrm{m\,s^{-2}}$
Mantle density	ρ_m	3400 $\mathrm{kg\,m^{-3}}$
Specific heat	C_p	1200 $\mathrm{J\,K^{-1}\,kg^{-1}}$
Thermal diffusivity	κ_0	10^{-6} $\mathrm{m^2\,s^{-1}}$
Thermal expansivity	α_0	3×10^{-5} $\mathrm{K^{-1}}$
Activation energy	E_a	157 $\mathrm{kJ\,mol^{-1}}$
Activation volume	V_a	5.69 $\mathrm{cm^3\,mol^{-1}}$
Latent heat of melting	L	640 $\mathrm{kJ\,kg^{-1}}$
Surface temperature	T_{surf}	220 K
Temperature difference across mantle	ΔT	1600 K
Rayleigh number	Ra	10^8

We use an activation energy of 157 kJ/mol for dislocation creep, but also run a simulation with an activation energy of 300 kJ/mol for diffusion creep, which may be more appropriate for Mars (*e.g.*, Grott and Breuer, 2009). For the higher activation energy run, we increase the Rayleigh number in order to obtain a similar viscosity profile (Fig. S1). We also run two simulations with a lower activation volume and higher Rayleigh number (Table 2).

Table 2. Simulation results.

Run	dcr **(km)**	κ_{ins}	Q_{ER}	**Non-default parameters**	tD1 **(Myr)**	tSP **(Myr)**
0	–	–	–	–	Never	Never
1	50	0.75	4	–	3.3	59
2	50	–	4	–	3.3	60
3	25	0.75	4	–	3.3	60
4	50	–	10	$d_{cr,N} = 25$ km, $Q_{ER,N} = 4$, $Q_{DE} = 0.5$	3.5	61
5	50	–	10	$d_{cr,N} = 25$ km, $Q_{ER,N} = 10$, $Q_{DE} = 0.5$	Never	Never
6	50	0.75	4	Impact heating ($R_i = 600$ km)	45[a]	60[a]
7	50	0.75	4	Impact heating ($R_i = 1200$ km)	63[a]	89[a]
8	50	0.75	4	$Ra = 2.39 \times 10^8$, $V_a = 4.65$ cm^3 mol^{-1}	3.5	67
9	50	0.75	4	$Ra = 2.39 \times 10^9$, $V_a = 4.65$ cm^3 mol^{-1}	2.6	16
10	50	–	4	$Ra = 1.52 \times 10^9$, $E_a = 300$ kJ mol^{-1}	43	158 (72)[b]

a. This is the time when degree-1 convection is dominant in the southern hemisphere. The initial impact heating perturbation causes earlier degree-1 patterns in the northern hemisphere.

b. Time in parentheses indicates when upwellings are concentrated in the southern hemisphere, but not yet a single plume.

We use a Rayleigh number of 10^8 which, given the parameters listed in Table 1, initial temperature profile, and temperature- and pressure-dependent viscosity, results in an average initial mantle viscosity of ~1.58×1021 Pa s (Fig. S1). Experiments have suggested viscosity variations of ~100–1000 across the sublithospheric mantle on Earth (Karato and Wu, 1993; Karato and Jung, 2003). The Martian mantle, presumably also primarily olivine, contains ~17 wt% FeO (Dreibus and Wanke, 1985) compared to ~8 wt% in the Earth's upper mantle (McDonough and Sun, 1995), which could reduce the viscosity of Mars' mantle by a factor of 10 relative to Earth's mantle (Zhao et al., 2009). Increased iron content could also result in a higher activation volume for the Martian mantle, leading to increased viscosity variations with depth (Raterron et al., 2017).

To simulate the effect of an initial crustal thickness variation caused by a Borealis-scale giant impact, we add a crustal cap of thickness dcr=25 or 50 km to the southern hemisphere. In CitcomS, this is accomplished by adding an insulating effect to elements in the upper 25 or 50 km of the computational mesh in the southern hemisphere. The insulating effect of the cap is parameterized using a reduction of thermal diffusivity κ0 by a factor κins and/or an enrichment in heat production *Q* by a factor QER (crustal thermal diffusivity κcr=κins·κ0and crustal heat production Qcr=QER·Q). We use a factor of 0.75 for κins, representing the difference between the thermal conductivity of 2–3 W m^{-1} K^{-1} for crustal rocks (Clauser and Huenges, 1995) and 4 W m^{-1} K^{-1} for mantle rock (Hofmeister, 1999), and the density difference between the crust and mantle. In some simulations we do not modify the diffusivity in the crust, to examine if a hemispherical difference in heat producing elements alone can drive degree-1 convection. Radiogenic-heat producing elements are preferentially partitioned into the crust, and we use a crustal enrichment factor QER=4 relative to the mantle, similar to the enrichment found at mid-ocean ridge basalts (Basaltic Volcanism Study Project, 1981). The northern hemisphere crust is excluded from most of our calculations because of its low volume and low concentration of heating elements relative to the southern crust. However, to examine the effect of including a thinner, less enriched northern crust, we complete a simulation (Run 4) in which we include a northern crust with thickness dcr,N=25 km and crustal enrichment factor QER,N=4, a southern crust of thickness dcr=50 km and crustal enrichment factor QER=10 (Taylor et al., 2006); both QER and QER,N are relative to the mantle, which in Runs 4 and 5 is depleted in radiogenic-heat producing elements by a factor QDE=0.5. We compare Run 4 to a case where both the northern and southern hemisphere have different thicknesses, but the same amount of radiogenic-heat producing elements (Run 5).

Melt production is computed during the simulation using the tracer method described in Li et al. (2016). The melt fraction (by mass) *F* is computed using the dry parameterization given by Katz et al. (2003). We extract melt when it exceeds a threshold value F>0.04. On Earth, the melt extraction threshold is between 1 and 4% (Li et al., 2016) (and references therein), and we expect a higher extraction threshold on Mars due to the lower gravity. Because the simulation is Boussinesq, we first add an adiabatic temperature gradient of 0.18 K km^{-1} before computing the melt fraction. We extract melt only at depths <540 km, where melt is buoyant on Mars (*e.g.*, Plesa et al., 2016, and references therein). The latent heat of melting is used as a temperature sink in Equation (3). We sum the melt production for elements in the uninsulated northern and insulated southern hemispheres to compute the cumulative melt production in each hemisphere over time. It is important to note that we do not consider the effects of crust production on the calculation itself (except for latent heating); crust produced in either hemisphere does not alter the crustal thickness/enrichment assumed at the start of the simulation.

Although impact heating from a giant impact is expected to dissipate relatively quickly (*e.g.*, Roberts and Arkani-Hamed, 2017) we test this by including localized impact heating in two of our simulations. We insert an initial temperature pulse from a giant impact using the method described in Golabek et al. (2011) (and references therein). We examine initial temperature perturbations from impactors of radius Rimp=600 and 1200 km. The resulting temperature perturbation roughly corresponds to a temperature increase of ~400 K within ~1.4Rimp of the impact site, radially decreasing in magnitude at further distances to <100 K at ~2Rimp from the impact site.

3. Results

The results for 11 simulations, including a control run, are reported in Table 2. We determine the time until degree-1 convection is reached, tD1, based on when the dominant spherical harmonic of the temperature in the lower, middle, and upper mantle are all degree-1. We also report the time that single plume convection, tSP, is achieved, based on when a clear single plume is visible extending through the entire mantle, centered under the insulating crust in the southern hemisphere. Run 0 is a control case with no insulating cap that never achieved degree-1 convection for the simulation duration (600 Myr).

We find that an insulating cap can induce degree-1 convection on relatively short timescales <100 Myr (Table 2). In most simulations, large single plumes are observed under the insulating southern crust in <100 Myr (Fig. 2). This occurs even when the thickness of the southern cap is reduced to 25 km (Run 3), and when there is only a change in enrichment factor, with no change in thermal diffusivity in the crust (Run 2). Simulations with initial impact heating included (Runs 6 and 7) still achieve degree-1 convection in under 100 Myr, showing that variations in crustal thickness and composition result in a single upwellingunder the insulating crust, even if earlier upwellings are concentrated under the impact site (Fig. 3). A lower activation volume (Run 8) slightly increases tSP, while a higher Rayleigh number (Run

9) decreases tSP to only 16 Myr. Use of a higher activation energy (Run 10) results in a longer timescale for single-plume convection (~160 Myr), although multiple plumes are still concentrated in the southern hemisphere in <75 Myr.

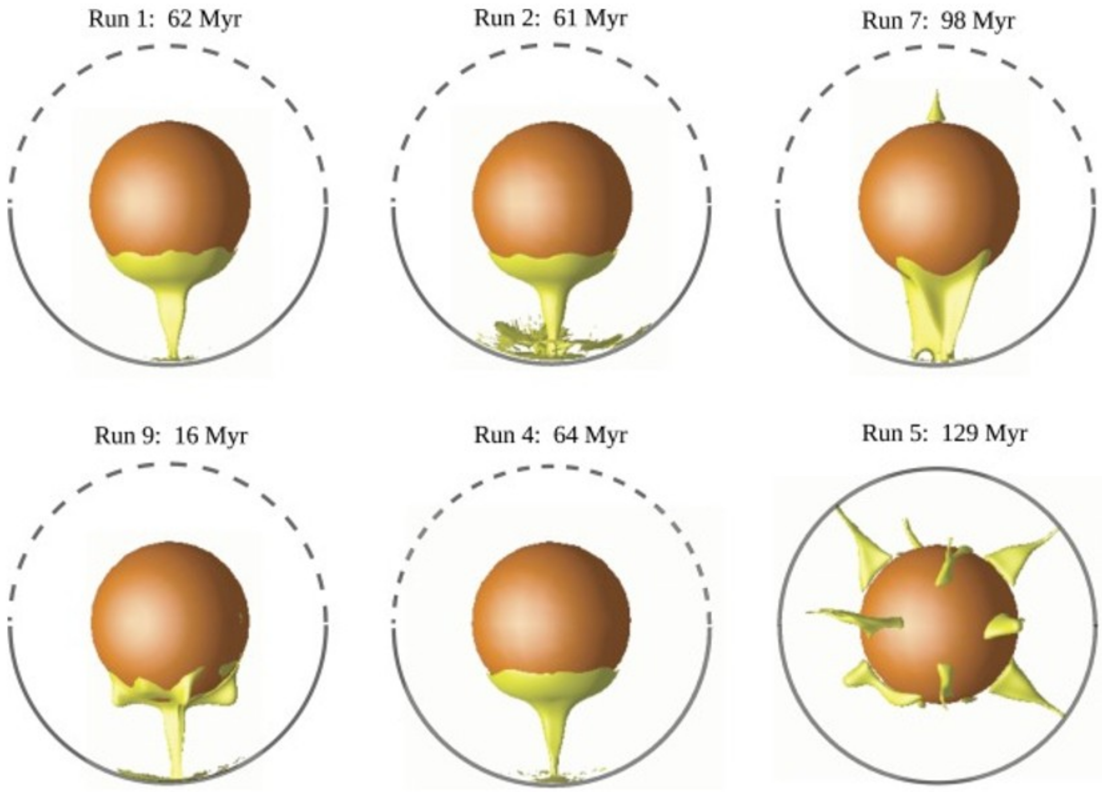

Fig. 2. Upwelling contours for residual temperature of 80 K, with the upper 100 km omitted for clarity. The southern crust (solid grey line) is enriched relative to the mantle and unenriched northern crust (dashed grey line). A single large upwelling under the insulating southern crust dominates the convection pattern in 10s to 100s of Myr. Run 7 has a residual lower mantle plume in the northern hemisphere, caused by the initial impact heating perturbation, but has still become dominated by degree-1 convection in <100 Myr. Run 9 uses a higher Rayleigh number and achieves single plume convection in ~16 Myr. In Run 4, both the northern and southern crusts are enriched by a factor of 4 and 10, respectively, relative to the mantle, and the upwelling concentrates under the more enriched and thicker southern crust. In Run 5, the northern and southern crusts are enriched by the same amount relative to the mantle, and no degree-1 convection pattern develops.

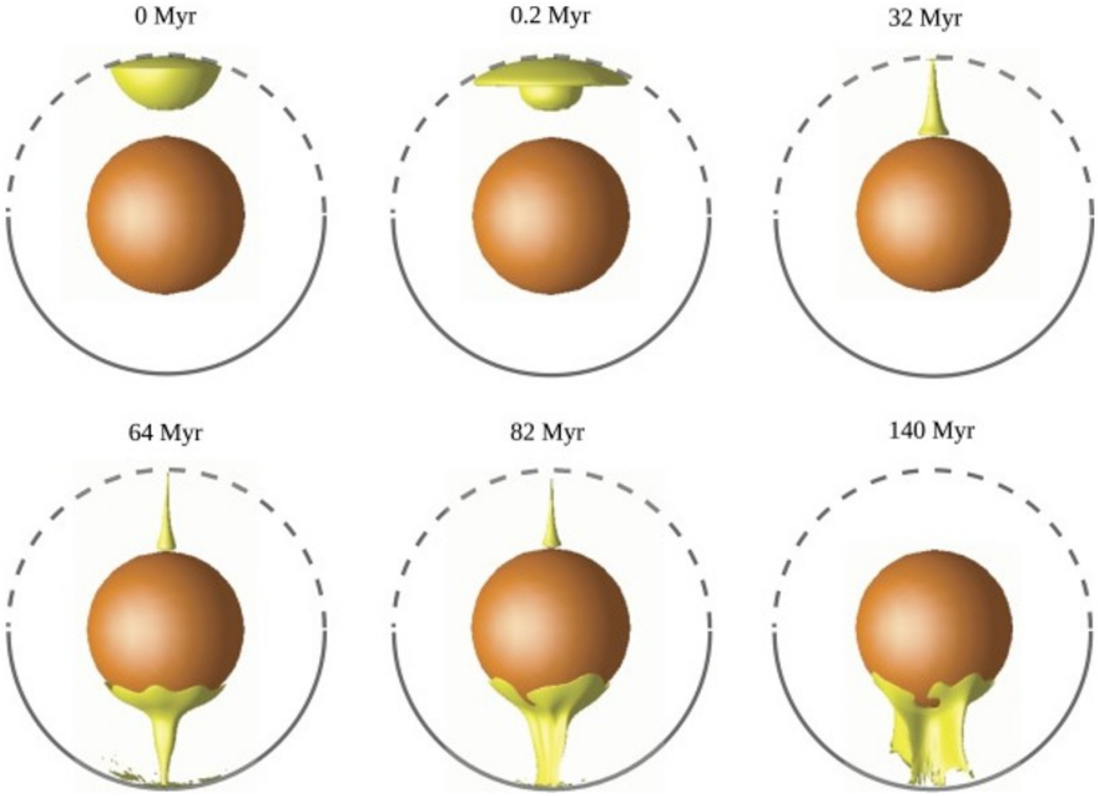

Fig. 3. Evolution of Run 6 over time. The simulation begins with a temperature perturbation from a giant impact in the northern hemisphere, which quickly dissipates and causes a short-lived northern upwelling. Over time, an upwelling develops in the southern hemisphere under the insulating crust, and the northern upwelling dissipates. The southern plume dominates the convection pattern after ~60 Myr. Upwelling contours are plotted for residual temperature = 80 K, with the upper 100 km omitted for clarity. The depleted northern crust and enriched southern crust are shown as dashed and solid gray lines, respectively.

We also include a crust in both the southern and northern hemispheres, and show that increased enrichment in the thicker southern crust relative to the thinner northern crust results in development of a superplume under the southern crust (Run 4), while equal enrichment in the northern and southern crusts results in no degree-1 convection and multiple plumes in both hemispheres (Run 5). The relative concentration of radiogenic-heat producing elements between the northern and southern crusts is the primary driver of degree-1 convection.

The focusing of upwelling(s) under the insulating cap increases melt production in the southern hemisphere (Fig. 4). In most simulations, a melt volume equivalent to 10–20 km of additional crust is produced in the insulated southern hemisphere. The amount of crust produced in the uninsulated northern hemisphere is negligible, except in simulations that begin with an impact heating perturbation (Runs 6 and 7). The crust production following impact heating is not expected to affect the overall result, because of its low volume/enrichment relative to the southern crust. For example, in Run 4 the simulation begins with 25 km of crust in the northern hemisphere (twice the thickness of northern crust produced in Runs 6 and 7), which is depleted relative to the more enriched southern crust, and a superplume still develops under the southern crust. In Runs 6 and 7, the cumulative crust production antipodal to the impact site eventually becomes greater than the northern, post-impact crust production, even for Rimp=1200 km, indicating that melt production in the southern hemisphere is enhanced by the increased vigor of the degree-1 upwelling (e.g., Fig. 3) and the increased subcrustal temperatures caused by the higher concentration of heating elements and decreased thermal diffusivity in the insulating cap.

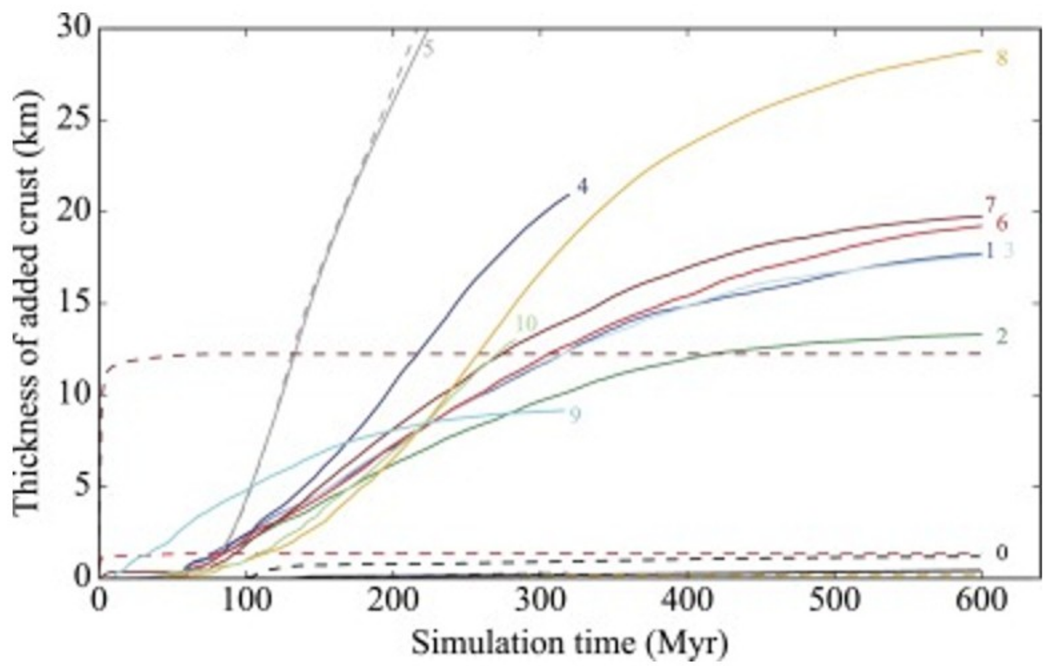

Fig. 4. The cumulative thickness of additional crust produced in the hemisphere with the insulated cap (solid lines) and the un-insulated hemisphere (dashed-lines). Run number is given next to the corresponding line. Thickness is computed by dividing the volume of melt production in each hemisphere by the surface area of each hemisphere. Crust production generally begins within the first 100 Myr, and continues for several hundred Myr before tapering off.

4. Discussion

The results of our simulations, particularly τSP and the crust production rate, could vary depending on mantle rheology, composition, and melting model. The use of a highly temperature-dependent viscosity promotes long-wavelength convection, because low viscosity layers below cold boundary layers (and above hot ones) reduce horizontal shear dissipation, allowing for longer wavelength cells (Lenardic et al., 2006). Similarly, the additional inclusion of a viscosity jump in the mantle (*e.g.*, Roberts and Zhong, 2006) would likely decrease τD1 and τSP. Inclusion of a non-newtonian rheology is not expected to have a significant effect on the vigor of convection on Mars (Hauck and Phillips, 2002), although it could raise mantle temperatures, allowing for enhanced partial melting even with a dry rheology (Grott and

Breuer, 2009). Phase transitions in the mid-mantle have been shown to have a weak effect on Martian mantle dynamics, and a perovskite + ferropericlase layer at the base of the mantle is unlikely (Ruedas et al., 2013). Partial melting and water content can also have significant effects for mantle convection on Mars (*e.g.*, Ruedas et al., 2013), motivating the use of more complex melting models that account for volatile depletion (*e.g.*, Li et al., 2016) or two-phase flow (*e.g.*, Dannberg and Heister, 2016). However, we do not expect the inclusion of more complex melting models to affect $\tau D1$, because most melt production occurs after degree-1 convection is achieved.

Cumulative crust production depends on the mantle composition and solidus (Kiefer et al., 2015), and the compressibility of melt extracted from depth (Dannberg and Heister, 2016). The solidus we use from Katz et al. (2003) is similar to other models of melting on Mars to the depths that we extract melt (Ruedas and Breuer, 2017), so a different solidus should not affect our results. Inclusion of two-phase flow and melt migration/depletion could affect plume dynamics (Dannberg and Heister, 2016) and alter the crustal thickness distribution due to lateral transport of melt below the surface, however, the different timescales over which melt and mantle materials flow makes it computationally expensive to couple the two processes in global simulations, and effects of two-phase flow are generally localized and should not affect the global convection/melting patterns we observe. Although different melting models would have variable effects on cumulative melt production, examining the full range of compositional considerations and variables such as melt extraction threshold is outside of the scope of this work. Effects that reduce crust production, such as permeability extraction barriers (Schools and Montési, 2018), could be compensated for with increased mantle temperature or higher initial water content (which may be the case for early Mars; *e.g.*, Wade et al., 2017). Thus, while more complex rheologies and melting models could affect crust production and $\tau D1$, we do not expect such considerations to alter our main conclusion that crustal heating/insulation promotes the development of degree-1 upwelling(s) and melt production under the thicker, enriched southern crust within 100s of Myr of a giant impact.

We show that for reasonable estimates of melt extraction, the additional crust produced in the southern hemisphere is within the constraints of Mars' inferred crustal thickness (*e.g.*, Neumann et al., 2004). Mars' crustal thickness may be lower or higher depending on the assumed density of the Martian crust. While Neumann et al. (2004) suggest an average crustal thickness of 45 km, a higher assumed crustal density (Wieczorek and Zuber, 2004; Baratoux et al., 2014; Plesa et al., 2016) could allow for an average crustal thickness up to 81 km. Likewise, lower (and possibly laterally varying) crustal densities could result in lower inferred crustal thicknesses (Goossens et al., 2017). Such considerations would result in varying constraints for crust production. In particular, higher assumed crustal thickness would increase the insulation and the melt production in our simulations. Higher crust production could be compensated for if a portion of the newly produced crust is subsequently recycled via delamination (*e.g.*, Rudnick, 1995).

Our model relies on a giant impact resulting in a northern crust depleted in radiogenic-heat producing elements relative to the older southern crust. It is important to note, however, that such a dichotomy in radiogenic-heat producing elements is not observed in gamma ray spectrometer measurements, which show little variation in Th and K abundance across the Martian surface (Taylor et al., 2006). Those measurements only sample the upper few tens of cm of regolith, and may not constrain the distribution of heat producing elements deeper in the crust (Plesa et al., 2016). Small differences in the distribution of K and Th may reflect different underlying compositions (*e.g.*, Karunatillake et al., 2007), but may also be explained by weathering and aqueous alteration (Dohm et al., 2009). Furthermore, observations suggest the southern crust is less dense than the northern crust (*e.g.*, Baratoux et al., 2014), implying a buried felsic component to the southern crust, which would be enriched in radiogenic-heat producing elements such as K.

The short timescale we find for the crust to control the convective pattern is consistent with estimates of the influencing timescale of crustal thickness variations on mantle flow. We estimate the timescale for changes in crustal thickness to influence temperature and hence flow, τ_{crust}, as the time it takes for a temperature anomaly to develop under the crust comparable to the temperature difference between a mantle plume and the surrounding mantle (~100 K). We compare the time-dependent temperature solution for a solid half-space with a constant heat production rate (Carslaw et al., 1959) for an uninsulated medium with $k=4\ W\,m^{-1}\,K^{-1}$ and $Q=7.4\times10^{-8}\ W\ m^{-3}$ (typical for the first 100s of Myr of Mars' history (Wanke and Dreibus, 1994)), and an insulated medium with $\kappa_{ins}=0.75$ and $Q_{ER}=4$. The time it takes for the temperature difference between the insulated and uninsulated medium at 50 km depth to reach 80 K yields $\tau_{crust}\sim37$ Myr. The timescale for temperature changes to influence flow, τ_{flow}, should scale as ~v/d, where *v* is the plume velocity and $d=R_p-R_c$. Determining a scaling relationship for velocity in a spherical shellthat is heated both from below and within is a challenge (Deschamps et al., 2012). We extrapolate the results of Weller et al. (2016), which scale fluid velocity versus $H_{int}Ra^{-1/3}$, to the values used in our simulations, which yields $v\sim30\ mm\ yr^{-1}$ and $\tau_{flow}\sim58$ Myr. It thus seems reasonable that variations in crustal thickness could influence the convective pattern on <100 Myr timescales.

While we do not include the production or effects of melt-residue in our model, lateral variations in lithosphere thickness and highly viscous melt residue have been shown to drive differential rotation of the Martian lithosphere, resulting in the migration of the Tharsis plume to the dichotomy boundary (Zhong, 2009; Šrámek and Zhong, 2010). Differential rotation of the lithosphere with respect to the plume occurs even if the lithosphere remains stationary (Zhong, 2009; Šrámek and Zhong, 2010). We expect the plume to migrate and the lithosphere to remain stationary, because the equatorial bulge should stabilize the planet against large scale true polar wander (Daradich et al., 2008). The likely pre-Tharsis rotation pole of Mars is only ~20∘ from the current pole, corresponding to the fossil bulge identified by Matsuyama and Manga (2010). We expect limited Tharsis-induced true polar wander to have occurred only after the plume migrated from the center of the Southern crust to emplace Tharsis at the dichotomy boundary. Migration of the Tharsis plume along such a track is evidenced by volcanic resurfacing and crustal thickening (Hynek et al., 2011; Cheung and King, 2014).

Because of the importance of giant impacts and mantle dynamics on planetary evolution, the origin of the crustal dichotomy is critical to understanding Mars' subsequent geophysical evolution. Both giant impacts and degree-1 convection have been proposed as a mechanism to produce an early hemispherical Martian dynamo (Stanley et al., 2008; Amit et al., 2011; Monteux et al., 2015). Various dynamo models can constrain and be constrained by the relation between the rate and distribution of crust production and the timescale of magnetic reversals (*e.g.*, Dietrich et al., 2015). Termination of the Martian dynamo could be modulated by the outgassing of mantle water over time (Sandu and Kiefer, 2012), which is related to the vigor of mantle convection and efficiency of melt production. The pattern and vigor of convection on early Mars could also have important implications for the compositional evolution of crust–mantle system (Grott et al., 2013), spatial and temporal variations in Martian lithosphere thickness (*e.g.*, Kiefer and Li, 2009), and volcanic outgassing (*e.g.*, Grott et al., 2011), in addition to the geophysical constraints discussed in Section 1.1.

5. Conclusion

Our simulations show that a natural consequence of a Borealis-scale giant impact is the development of single-plume convection and significant melting in the southern hemisphere. This hybrid model is consistent with many of the geophysical observations related to crustal dichotomy formation. The formation of upwellings antipodal to the impact site allows for the preservation of the elliptical dichotomy boundary from a giant impact. Development of degree-1 convection in the southern hemisphere is rapid (<100 Myr), and could produce sufficient additional melt to further thicken the southern crust by ~10–20 km, due to both the increased vigor of the degree-1 upwelling and the increased subcrustal heating caused by the insulating effect of the thicker southern crust. The short timescale in which additional crust is produced (within 100s of Myr of Mars' formation) can explain the formation of strong remanent crustal magnetic signatures in the southern hemisphere before the end of the Martian dynamo. Depending on the extent of crust production, extraction of melt to the surface could leave sufficient highly viscous melt residue under the southern crust to induce plume migration (Zhong, 2009; Šrámek and Zhong, 2010), resulting in the formation of Tharsis on the dichotomy boundary. The hybrid model for dichotomy formation can therefore bridge the gap between an early Borealis impact 4.5 Ga (Bottke and Andrews-Hanna, 2017) and a late Noachian formation of Tharsis >3.7 Ga (*e.g.*, Bouley et al., 2016), with broad implications for the geophysical evolution of Mars.

Acknowledgments

We thank Mingming Li for providing the melting subroutines for CitcomS and for helpful discussions. R.C. was supported by NSFEAR-1135382. This work used the Savio computational cluster resource provided by the Berkeley Research Computing program at the University of California, Berkeley (supported by the UC Berkeley Chancellor, Vice Chancellor for Research, and Chief Information Officer), the Extreme Science and Engineering Discovery Environment (XSEDE) (supported by National Science Foundationgrant number ACI-1053575), and resources of the National Energy Research Scientific Computing Center, a DOE Office of Science User Facility (supported by the Office of Science of the U.S. Department of Energy under Contract No. DE-AC02-05CH11231). CitcomS is available through the Computational Infrastructure for Geodynamics(geodynamics.org). We thank reviewer A.C. Barr, one anonymous reviewer, and editor W.B. McKinnon for comments and suggestions that clarified the presentation and refined the models.

References

Acuna et al., 1999

M.H. Acuna, J.E.P. Connerney, N.F. Ness, R.P. Lin, D. Mitchell, C.W. Carlson, J. McFadden, K.A. Anderson, H. Reme, C. Mazelle, D. Vignes, P. Wasilewski, P. C loutier**Global distribution of crustal magnetization discovered by the Mars global surveyor MAG/ER experiment**

Science, 284 (5415) (1999), pp. 790-793

Amit et al., 2011

H. Amit, U.R. Christensen, B. Langlais**The influence of degree-1 mantle heterogeneity on the past dynamo of Mars**

Phys. Earth Planet. Inter., 189 (1–2) (2011), pp. 63-79

Andrews-Hanna et al., 2008

J.C. Andrews-Hanna, M.T. Zuber, W.B. Banerdt**The Borealis basin and the origin of the martian crustal dichotomy**

Nature, 453 (7199) (2008), pp. 1212-1215

Baratoux et al., 2014

D. Baratoux, H. Samuel, C. Michaut, M.J. Toplis, M. Monnereau, M. Wieczorek, R. Garcia, K. Kurita**Petrological constraints on the density of the Martian crust**

J. Geophys. Res., Planets, 119 (7) (2014), pp. 1707-1727

Basaltic Volcanism Study Project, 1981

Basaltic Volcanism Study Project**Basaltic Volcanism on the Terrestrial Planets**

Pergamon Press, New York (1981)

Bottke and Andrews-Hanna, 2017

W.F. Bottke, J.C. Andrews-Hanna**A post-accretionary lull in large impacts on early Mars**

Nat. Geosci., 10 (5) (2017), pp. 344-348

Bouley et al., 2016

S. Bouley, D. Baratoux, I. Matsuyama, F. Forget, A. Séjourné, M. Turbet, F. Costard**Late Tharsis formation and implications for early Mars**

Nature, 531 (7594) (2016), pp. 344-347

Brasser and Mojzsis, 2017

R. Brasser, S.J. Mojzsis**A colossal impact enriched Mars' mantle with noble metals**

Geophys. Res. Lett., 44 (12) (2017), pp. 5978-5985

Carslaw et al., 1959

H.S.S. Carslaw, J.C. Jaeger, J.C. Jaeger**Conduction of Heat in Solids**

(2nd edition), Clarendon Press, Oxford (1959)

Cheung and King, 2014

K.K. Cheung, S.D. King**Geophysical evidence supports migration of Tharsis volcanism on Mars**

J. Geophys. Res., Planets, 119 (5) (2014), pp. 1078-1085

Citron and Zhong, 2012

R.I. Citron, S. Zhong**Constraints on the formation of the Martian crustal dichotomy from remnant crustal magnetism**

Phys. Earth Planet. Inter., 212–213 (2012), pp. 55-63

Clauser and Huenges, 1995

C. Clauser, E. Huenges**Thermal conductivity of rocks and minerals**

T.J. Ahrens (Ed.), Rock Physics and Phase Relations: A Handbook of Physical Constants, AGU Ref. Shelf, vol. 3, AGU, Washington DC (1995), pp. 105-126

Collins et al., 2011

G.S. Collins, D. Elbeshausen, T.M. Davison, S.J. Robbins, B.M. Hynek**The size-frequency distribution of elliptical impact craters**

Earth Planet. Sci. Lett., 310 (1–2) (2011), pp. 1-8

Connerney et al., 2005

J.E.P. Connerney, M.H. Acuña, N.F. Ness, G. Kletetschka, D.L. Mitchell, R.P. Lin , H.Reme**Tectonic implications of Mars crustal magnetism**

Proc. Natl. Acad. Sci. USA, 102 (2005), pp. 14970-14975

Dannberg and Heister, 2016

J. Dannberg, T. Heister**Compressible magma/mantle dynamics: 3-D, adaptive simulations in ASPECT**

Geophys. J. Int., 207 (3) (2016), pp. 1343-1366

Daradich et al., 2008

A. Daradich, J.X. Mitrovica, I. Matsuyama, J.T. Perron, M. Manga, M.A. Richard s**Equilibrium rotational stability and figure of Mars**

Icarus, 194 (2) (2008), pp. 463-475

Deschamps et al., 2012

F. Deschamps, C. Yao, P.J. Tackley, C. Sanchez-Valle**High Rayleigh number thermal convection in volumetrically heated spherical shells**

J. Geophys. Res. E, Planets, 117 (9) (2012), pp. 1-12

Dietrich et al., 2015

W. Dietrich, J. Wicht, K. Hori**Effect of width, amplitude, and position of a core mantle boundary hot spot on core convection and dynamo action**

Prog. Earth Planet. Sci., 2 (1) (2015), p. 35

Dohm et al., 2009

J.M. Dohm, V.R. Baker, W.V. Boynton, A.G. Fairén, J.C. Ferris, M. Finch, R. Furf aro, T.M.Hare, D.M. Janes, J.S. Kargel, S. Karunatillake, J. Keller, K. Kerry, K.J. Kim, G. Komatsu, W.C. Mahaney, D. Schulze-Makuch, L. Marinangeli, G.G. Ori, J. Ruiz, S.J. Wheelock**GRS evidence and the possibility of paleooceans on Mars**

Planet. Space Sci., 57 (5–6) (2009), pp. 664-684

Dreibus and Wanke, 1985

G. Dreibus, H. Wanke**Mars, a volatile-rich planet**

Meteoritics, 20 (1985), pp. 367-381

Elkins-Tanton et al., 2005

L.T. Elkins-Tanton, S.E. Zaranek, E.M. Parmentier, P.C. Hess**Early magnetic field and magmatic activity on Mars from magma ocean cumulate overturn**

Earth Planet. Sci. Lett., 236 (1–2) (2005), pp. 1-12

Frey, 2006

H.V. Frey**Impact constraints on, and a chronology for, major events in early Mars history**

J. Geophys. Res. E, Planets, 111 (8) (2006), pp. 1-11

Golabek et al., 2018

G.J. Golabek, A. Emsenhuber, M. Jutzi, E.I. Asphaug, T.V. Gerya**Coupling SPH and thermochemical models of planets: methodology and example of a Mars-sized body**

Icarus, 301 (2018), pp. 235-246

Golabek et al., 2011

G.J. Golabek, T. Keller, T.V. Gerya, G. Zhu, P.J. Tackley, J.a.D. Connolly**Origin of the martian dichotomy and Tharsis from a giant impact causing massive magmatism**

Icarus, 215 (1) (2011), pp. 346-357

Goossens et al., 2017

S. Goossens, T.J. Sabaka, A. Genova, E. Mazarico, J.B. Nicholas, G.A. Neuman n**Evidence for a low bulk crustal density for Mars from gravity and topography**

Geophys. Res. Lett., 44 (15) (2017), pp. 7686-7694

Grott et al., 2013

M. Grott, D. Baratoux, E. Hauber, V. Sautter, J. Mustard, O. Gasnault, S.W. Ru ff, S.I. Karato, V.Debaille, M. Knapmeyer, F. Sohl, T. van Hoolst, D. Breuer, A. Morschhauser, M.J. Toplis**Long-term evolution of the martian crust–mantle system**

Space Sci. Rev., 174 (2013), pp. 49-111

Grott and Breuer, 2009

M. Grott, D. Breuer**Implications of large elastic thicknesses for the composition and current thermal state of Mars**

Icarus, 201 (2) (2009), pp. 540-548

Grott et al., 2011

M. Grott, A. Morschhauser, D. Breuer, E. Hauber**Volcanic outgassing of CO_2 and H_2O on Mars**

Earth Planet. Sci. Lett., 308 (3–4) (2011), pp. 391-400

Gurnis, 1988

M. Gurnis**Large-scale mantle convection and the aggregation and dispersal of supercontinents**

Nature, 332 (6166) (1988), pp. 695-699

Harder, 2000

H. Harder**Mantle convection and the dynamic geoid of Mars**

Geophys. Res. Lett., 27 (3) (2000), pp. 301-304

Hauck and Phillips, 2002

S.A. Hauck, R.J. Phillips**Thermal and crustal evolution of Mars**

J. Geophys. Res., 107 (E7) (2002), Article 5052

Hofmeister, 1999

A.M. Hofmeister**Mantle values of thermal conductivity and the geotherm from phonon lifetimes**

Science, 283 (1999), pp. 1699-1706

Hynek et al., 2011

B.M. Hynek, S.J. Robbins, O. Šrámek, S.J. Zhong**Geological evidence for a migrating Tharsis plume on early Mars**

Earth Planet. Sci. Lett., 310 (2011), pp. 327-333

Karato and Jung, 2003

S.-I. Karato, H. Jung**Effects of pressure on high-temperature dislocation creep in olivine**

Philos. Mag., 83 (3) (2003), pp. 401-414

Karato and Wu, 1993

S. Karato, P. Wu**Rheology of the upper mantle: a synthesis**

Science, 260 (5109) (1993), pp. 771-778

Karunatillake et al., 2007

S. Karunatillake, S.W. Squyres, G.J. Taylor, J.M. Keller, O. Gasnault, L.G. Evans , R.C.Reedy, R.D. Starr, W.V. Boynton, D.M. Janes, K.E. Kerry, J.M. Dohm, A.L. Sprague, B.C. Hahn, D.Hamara**Composition of northern low-albedo regions of Mars: insights from the Mars Odyssey Gamma Ray Spectrometer**

J. Geophys. Res. E, Planets, 112 (3) (2007), pp. 1-16

Katz et al., 2003

R.F. Katz, M. Spiegelman, C.H. Langmuir**A new parameterization of hydrous mantle melting**

Geochem. Geophys. Geosyst., 4 (9) (2003), pp. 1-19

Keller and Tackley, 2009

T. Keller, P.J. Tackley**Towards self-consistent modeling of the martian dichotomy: the influence of one-ridge convection on crustal thickness distribution**

Icarus, 202 (2) (2009), pp. 429-443

Kiefer, 2005

W.S. Kiefer**Buried mass anomalies along the hemispheric dichotomy in eastern Mars: implications for the origin and evolution of the dichotomy**

Geophys. Res. Lett., 32 (22) (2005), pp. 1-4

Kiefer et al., 2015

W.S. Kiefer, J. Filiberto, C. Sandu, Q. Li**The effects of mantle composition on the peridotite solidus: implications for the magmatic history of Mars**

Geochim. Cosmochim. Acta, 162 (2015), pp. 247-258

Kiefer and Li, 2009

W.S. Kiefer, Q. Li**Mantle convection controls the observed lateral variations in lithospheric thickness on present-day Mars**

Geophys. Res. Lett., 36 (18) (2009), Article L18203

Lenardic et al., 2006

A. Lenardic, M.A. Richards, F.H. Busse**Depth-dependent rheology and the horizontal length scale of mantle convection**

J. Geophys. Res., 111 (B7) (2006), Article B07404

Li et al., 2016

M. Li, B. Black, S. Zhong, M. Manga, M.L. Rudolph, P. Olson**Quantifying melt production and degassing rate at mid-ocean ridges from global mantle convection models with plate motion history**

Geochem. Geophys. Geosyst., 17 (7) (2016), pp. 2884-2904

Lillis et al., 2013

R.J. Lillis, S. Robbins, M. Manga, J.S. Halekas, H.V. Frey**Time history of the Martian dynamo from crater magnetic field analysis**

J. Geophys. Res., Planets, 118 (7) (2013), pp. 1488-1511

Marinova et al., 2008

M.M. Marinova, O. Aharonson, E. Asphaug**Mega-impact formation of the Mars hemispheric dichotomy**

Nature, 453 (June 2008), pp. 1216-1219

Matsuyama and Manga, 2010

I. Matsuyama, M. Manga**Mars without the equilibrium rotational figure, Tharsis, and the remnant rotational figure**

J. Geophys. Res., Planets, 115 (12) (2010), Article E12020, 10.1029/2010JE003686

McDonough and Sun, 1995

W.F. McDonough, S.-s. Sun**The composition of the Earth**

Chem. Geol., 120 (1995), pp. 223-253

Monteux et al., 2015

J. Monteux, H. Amit, G. Choblet, B. Langlais, G. Tobie**Giant impacts, heterogeneous mantle heating and a past hemispheric dynamo on Mars**

Phys. Earth Planet. Inter., 240 (2015), pp. 114-124

Neumann et al., 2004

G.A. Neumann, M.T. Zuber, M.A. Wieczorek, P.J. McGovern, F.G. Lemoine, D.E. Smith**Crustal structure of Mars from gravity and topography**

J. Geophys. Res., Planets, 109 (8) (2004), pp. 1-18

Nimmo et al., 2008

F. Nimmo, S.D. Hart, D.G. Korycansky, C.B. Agnor**Implications of an impact origin for the martian hemispheric dichotomy**

Nature, 453 (2008), pp. 1220-1223, 10.1038/nature07025

Nimmo and Tanaka, 2005

F. Nimmo, K. Tanaka**Early crustal evolution of Mars**

Annu. Rev. Earth Planet. Sci., 33 (1) (2005), pp. 133-161

Plesa and Breuer, 2014

A.C. Plesa, D. Breuer**Partial melting in one-plate planets: implications for thermo-chemical and atmospheric evolution**

Planet. Space Sci., 98 (2014), pp. 55-65

Plesa et al., 2016

A.-C. Plesa, M. Grott, N. Tosi, D. Breuer, T. Spohn, M.A. Wieczorek**How large are present-day heat flux variations across the surface of Mars?**

J. Geophys. Res., Planets, 121 (12) (2016), pp. 2386-2403

Raterron et al., 2017

P. Raterron, C. Holyoke, L. Tokle, N. Hilairet, S. Merkel, G. Hirth, D. Weidner**Effect of iron content on olivine viscosity and implications for the Martian mantle**

Lunar and Planetary Science XLVIII (2017), p. 1553

Roberts and Arkani-Hamed, 2017

J. Roberts, J. Arkani-Hamed**Effects of basin-forming impacts on the thermal evolution and magnetic field of Mars**

Earth Planet. Sci. Lett., 478 (2017), pp. 192-202

Roberts and Zhong, 2006

J.H. Roberts, S. Zhong**Degree-1 convection in the Martian mantle and the origin of the hemispheric dichotomy**

J. Geophys. Res., Planets, 111 (6) (2006), Article E06013

Rosenblatt et al., 2016

P. Rosenblatt, S. Charnoz, K.M. Dunseath, M. Terao-Dunseath, A. Trinh, R. Hyodo, H.Genda, S. Toupin**Accretion of Phobos and Deimos in an extended debris disc stirred by transient moons**

Nat. Geosci., 9 (August 2016), pp. 4-8

Rudnick, 1995

R.L. Rudnick**Making continental crust**

Nature, 378 (6557) (1995), pp. 571-578

Ruedas and Breuer, 2017

T. Ruedas, D. Breuer**On the relative importance of thermal and chemical buoyancy in regular and impact-induced melting in a Mars-like planet**

J. Geophys. Res., Planets, 122 (7) (2017), pp. 1554-1579

Ruedas et al., 2013

T. Ruedas, P.J. Tackley, S.C. Solomon**Thermal and compositional evolution of the martian mantle: effects of water**

Phys. Earth Planet. Inter., 220 (2013), pp. 50-72

Sandu and Kiefer, 2012

C. Sandu, W.S. Kiefer**Degassing history of Mars and the lifespan of its magnetic dynamo**

Geophys. Res. Lett., 39 (3) (2012), Article L03201

Scheinberg et al., 2014

A. Scheinberg, L.T. Elkins-Tanton, S.J. Zhong**Timescale and morphology of Martian mantle overturn immediately following magma ocean solidification**

J. Geophys. Res., Planets, 119 (3) (2014), pp. 454-467

Schools and Montési, 2018

J.W. Schools, L.G. Montési**The generation of barriers to melt ascent in the Martian lithosphere**

J. Geophys. Res., Planets, 123 (2018), pp. 47-66

Sekhar and King, 2014

P. Sekhar, S.D. King**3D spherical models of Martian mantle convection constrained by melting history**

Earth Planet. Sci. Lett., 388 (2014), pp. 27-37

Šrámek and Zhong, 2010

O. Šrámek, S. Zhong**Long-wavelength stagnant lid convection with hemispheric variation in lithospheric thickness: link between Martian crustal dichotomy and Tharsis?**

J. Geophys. Res., Planets, 115 (2010), pp. 1-20

Šrámek and Zhong, 2012

O. Šrámek, S. Zhong**Martian crustal dichotomy and Tharsis formation by partial melting coupled to early plume migration**

J. Geophys. Res., Planets, 117 (1) (2012), pp. 1-14

Stanley et al., 2008

S. Stanley, L. Elkins-Tanton, M.T. Zuber, E.M. Parmentier**Mars' paleomagnetic field as the result of a single-hemisphere dynamo**

Science, 321 (5897) (2008), pp. 1822-1825

Tan et al., 2006

E. Tan, E. Choi, P. Thoutireddy, M. Gurnis, M. Aivazis**GeoFramework: coupling multiple models of mantle convection within a computational framework**

Geochem. Geophys. Geosyst., 7 (6) (2006), Article Q06001

Taylor et al., 2006

G.J. Taylor, W.V. Boynton, J. Brückner, H. Wänke, G. Dreibus, K.E. Kerry, J.M. Keller, R.C.Reedy, L.G. Evans, R.D. Starr, S.W. Squyres, S. Karunatillake, O. Gasnault, S. Maurice, C. D'Uston, P.Englert, J.M. Dohm, V. Baker, D. Hamara, D. M. Janes, A.L. Sprague, K.J. Kim, D. Drake**Bulk composition and early differentiation of Mars**

J. Geophys. Res., Planets, 112 (3) (2006), Article E03S10

Wade et al., 2017

J. Wade, B. Dyck, R.M. Palin, J.D.P. Moore, A.J. Smye**The divergent fates of primitive hydrospheric water on Earth and Mars**

Nature, 552 (7685) (2017), pp. 391-394

Wanke and Dreibus, 1994

H. Wanke, G. Dreibus**Chemistry and accretion history of Mars**

Philos. Trans. R. Soc. Lond., Math. Phys. Eng. Sci., 349 (1690) (1994), pp. 285-293

Weller et al., 2016

M.B. Weller, A. Lenardic, W.B. Moore**Scaling relationships and physics for mixed heating convection in planetary interiors: isoviscous spherical shells**

J. Geophys. Res., Solid Earth, 121 (10) (2016), pp. 7598-7617

Wenzel et al., 2004

M.J. Wenzel, M. Manga, A.M. Jellinek**Tharsis as a consequence of Mars' dichotomy and layered mantle**

Geophys. Res. Lett., 31 (4) (2004), Article L04702

Wieczorek and Zuber, 2004

M.A. Wieczorek, M.T. Zuber**Thickness of the Martian crust: improved constraints from geoid-to-topography ratios**

J. Geophys. Res., 109 (E1) (2004), Article E01009

Zhao et al., 2009

Y.H. Zhao, M.E. Zimmerman, D.L. Kohlstedt**Effect of iron content on the creep behavior of olivine, 1: anhydrous conditions**

Earth Planet. Sci. Lett., 287 (1–2) (2009), pp. 229-240

Zhong, 2009

S. Zhong**Migration of Tharsis volcanism on Mars caused by differential rotation of the lithosphere**

Nat. Geosci., 2 (1) (2009), pp. 19-23

Zhong et al., 2000

S. Zhong, M.T. Zuber, L. Moresi, M. Gurnis**Role of temperature-dependent viscosity and surface plates in spherical shell models of mantle convection**

J. Geophys. Res., Solid Earth, 105 (B5) (2000), pp. 11063-11082